Supporting information

Generation mechanism of the defects in g-C_3N_4 synthesized in N_2 atmosphere and the method for improving photocatalysis activity

Xinye Chang [1], Huiqing Fan [1]*, Lin Lei [1], Xiaobo Wu [1], Weijia Wang [1]* and Longtao Ma [2]*

[1] State Key Laboratory of Solidification Processing, School of Materials Science and Engineering, Northwestern Polytechnical University, Xi'an 710072, China; xinyechang@163.com (X.C.); 15123812005@163.com (L.L.); xiaobo_wu2000@163.com (X.W.)

[2] Institute of Flexible Electronics, Northwestern Polytechnical University, Xi'an 710072, China

* Correspondence: hqfan@nwpu.edu.cn (H. F.); weijia.wang@nwpu.edu.cn (W. W.); iamltma@nwpu.edu.cn (L. M.)

Results and discussion (Figure S1-S7 and Table S1-S2)

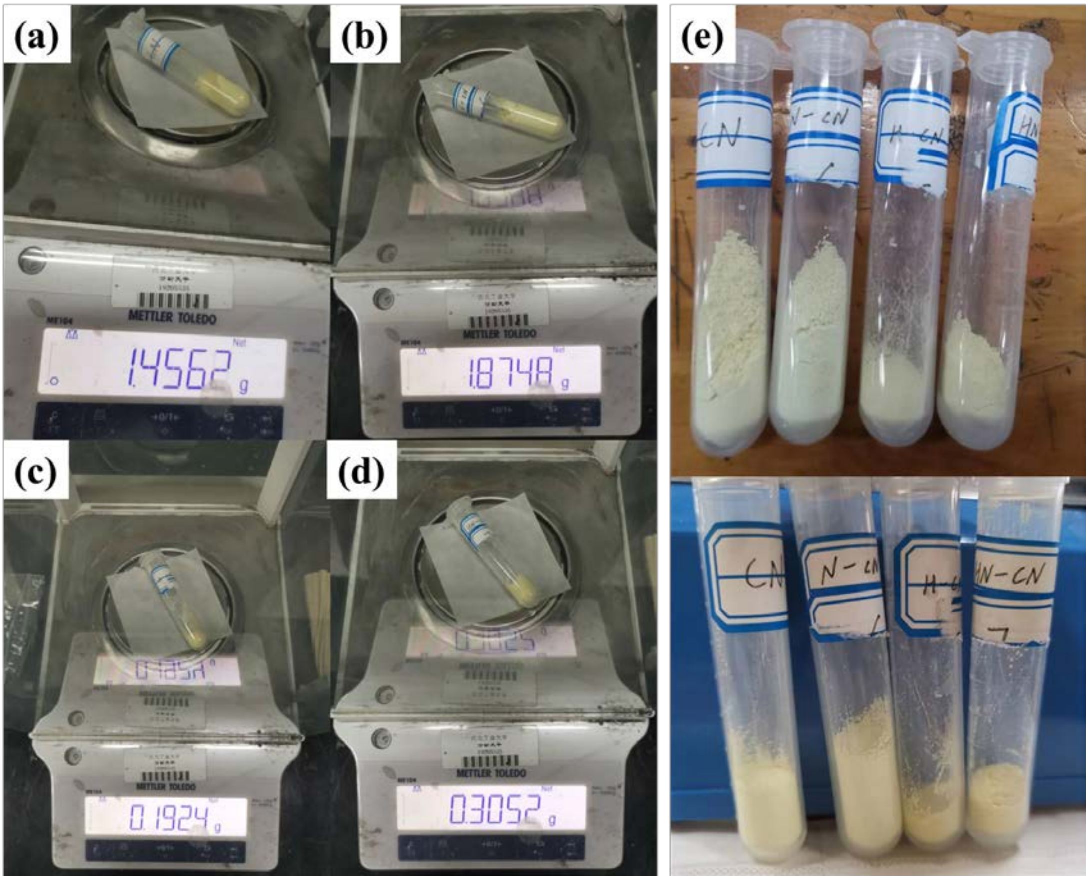

Figure S1. The weight of CN (a), N-CN (b), H-CN (c), and HN-CN(d), and their volume comparison (e).

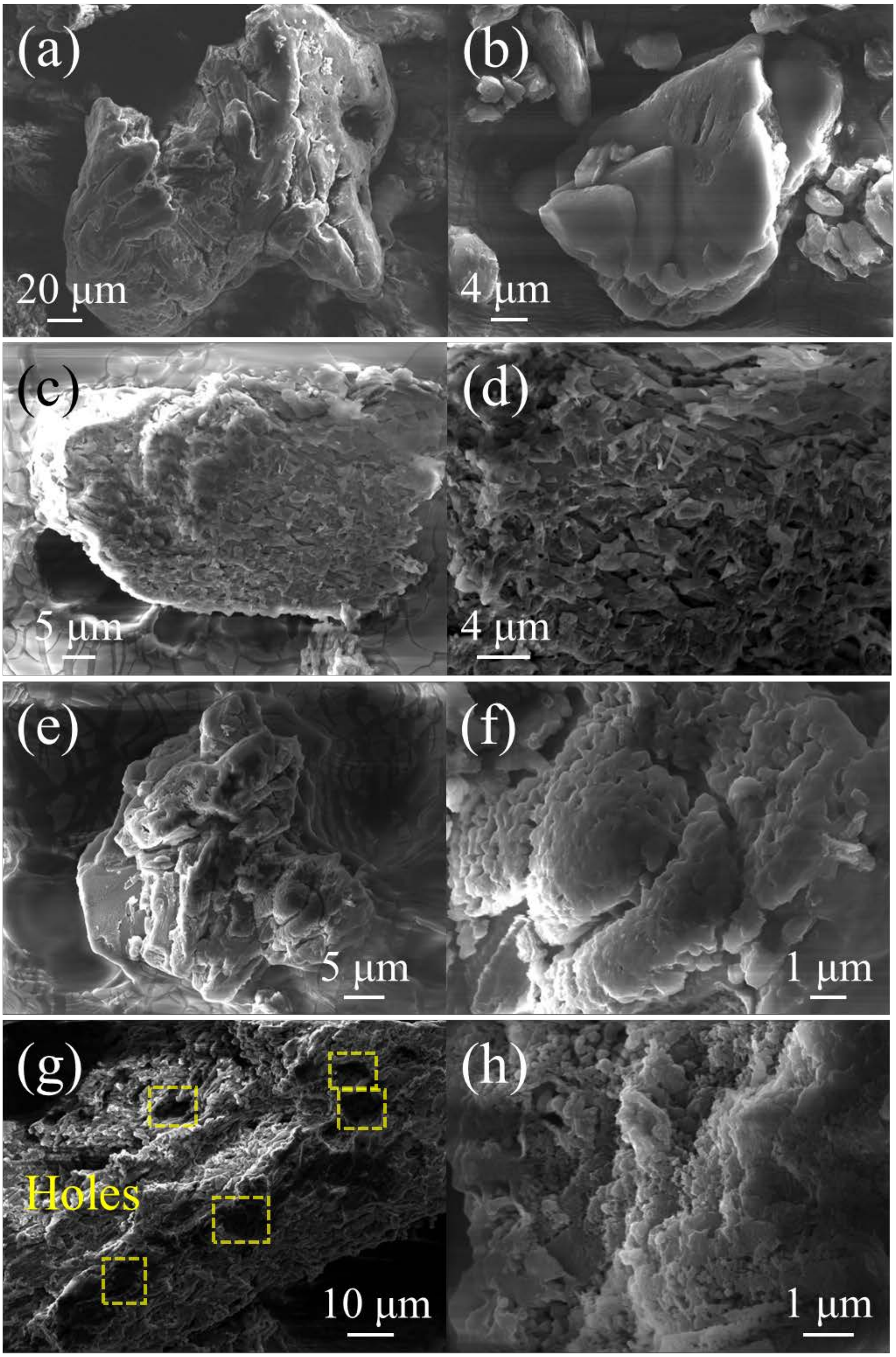

Figure S2. SEM images of CN (a) (b), H-CN (c) (d), N-CN (e) (f), and HN-CN (g) (h).

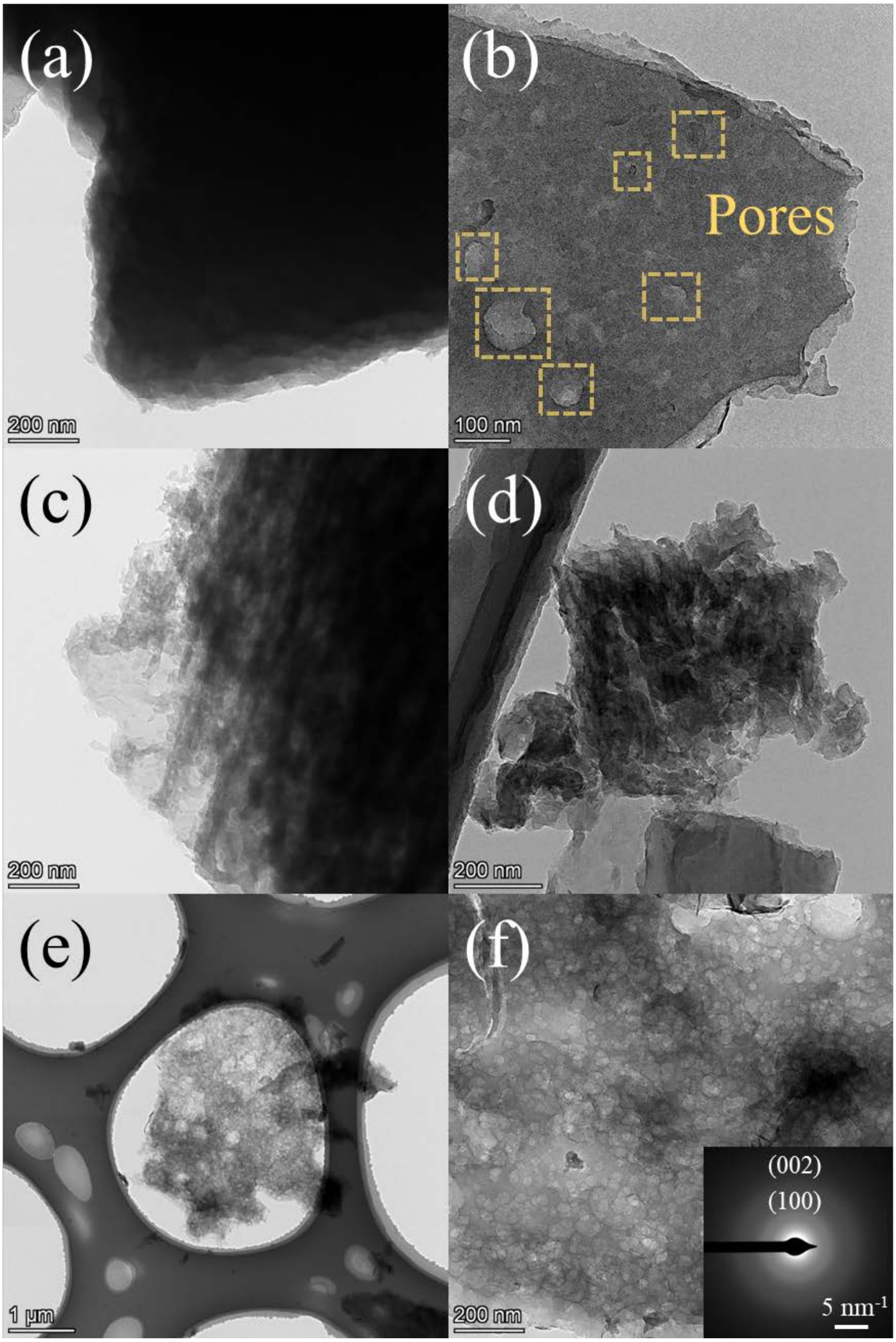

Figure S3. TEM images of CN (a), H-CN (b), N-CN (c) (d), and HN-CN (e) (f). Inset in (f) is the SAED pattern.

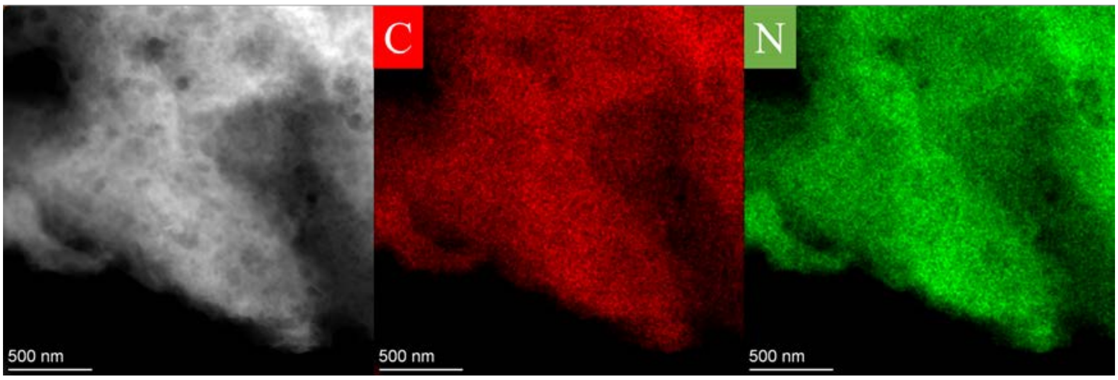

Figure S4. EDS elemental mapping patterns of HN-CN.

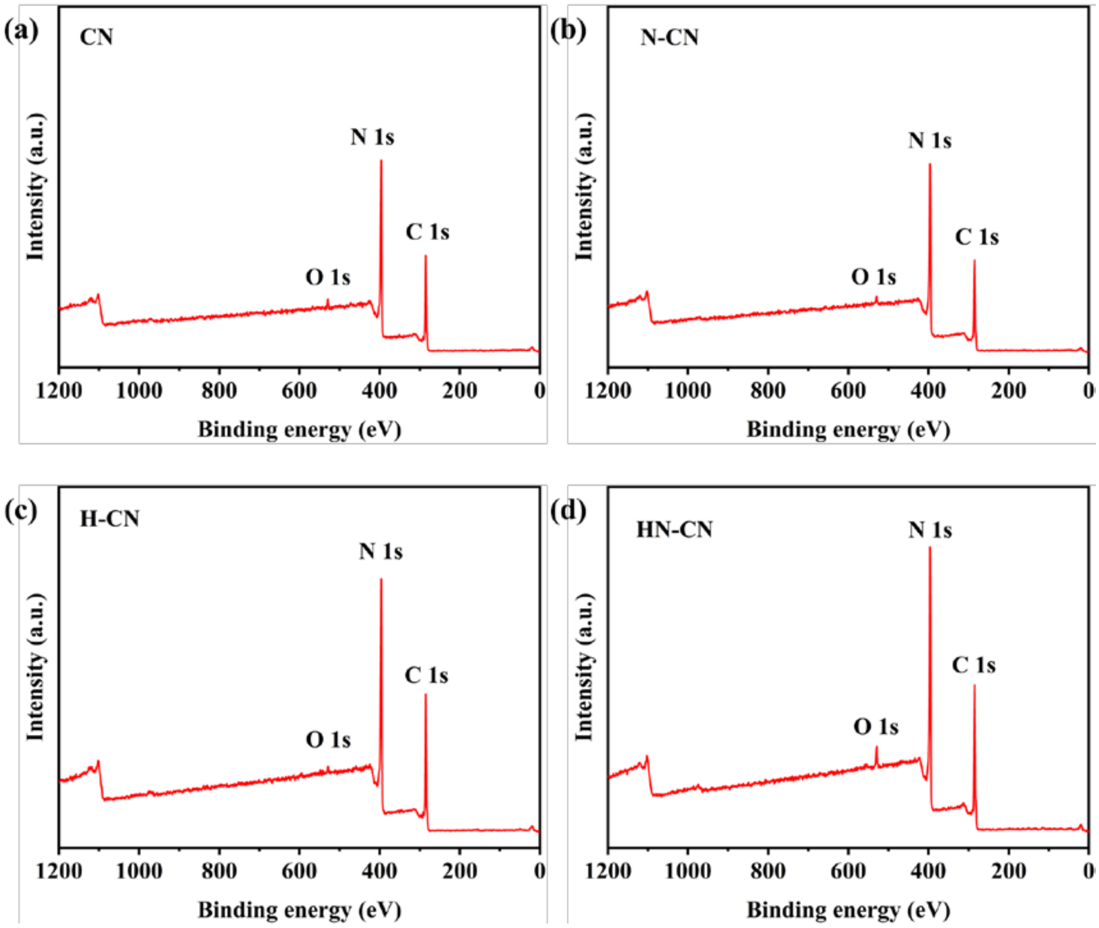

Figure S5. XPS survey spectrum of CN (a), N-CN (b), H-CN (c), and HN-CN (d).

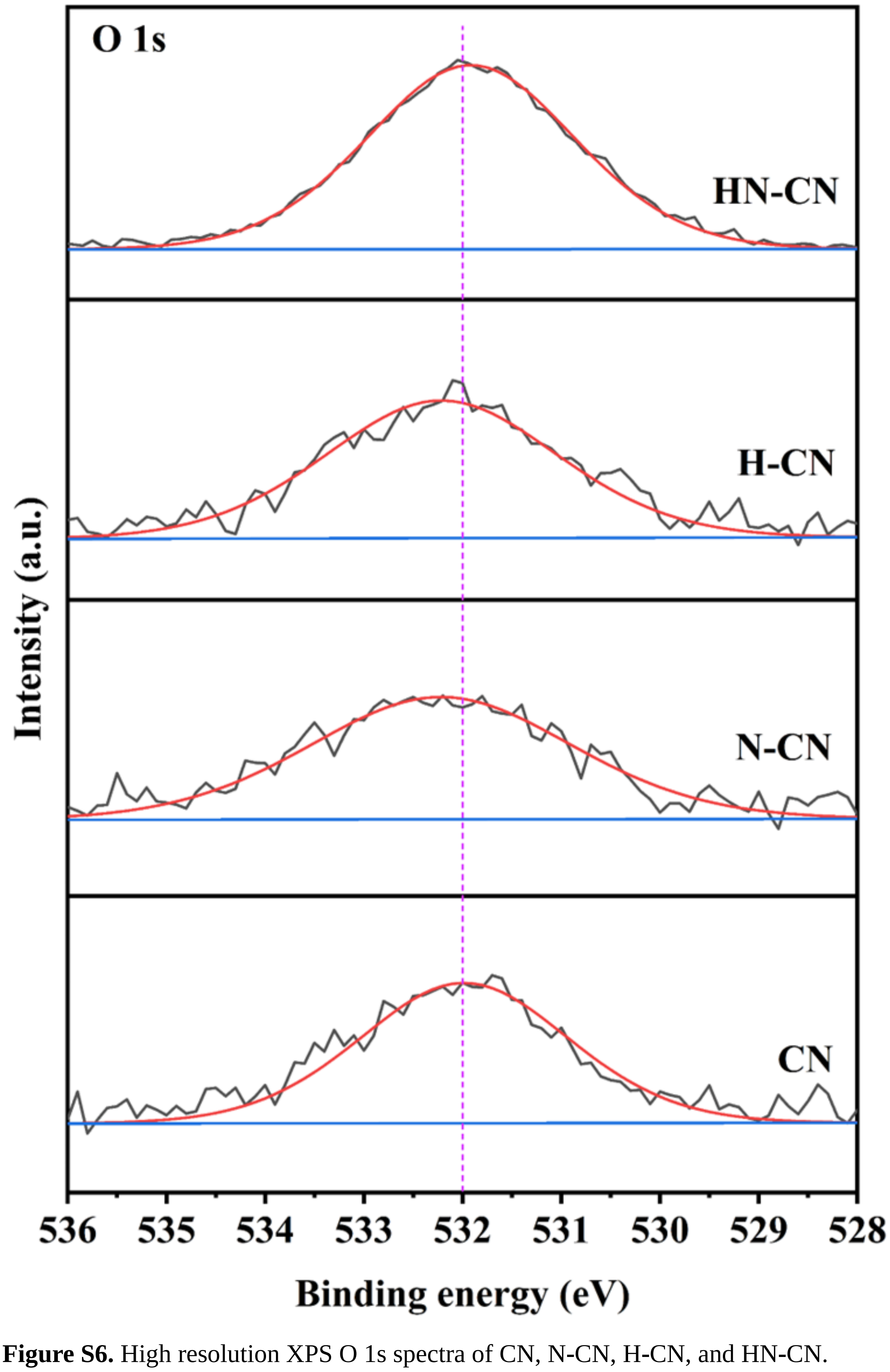

Figure S6. High resolution XPS O 1s spectra of CN, N-CN, H-CN, and HN-CN.

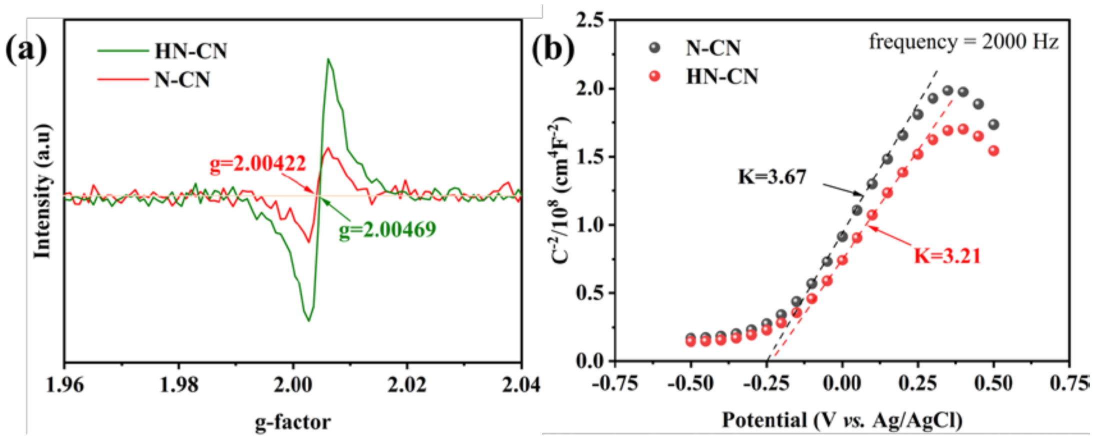

Figure S7. (a) EPR g-factor and (b) Mott-Schottky curves of N-CN and HN-CN.

The Lande factor (g) can be calculated using the following equations:

$$g = \frac{h\nu}{\beta H} \tag{1}$$

where h is Planck constant, ν is microwave frequency, β is Bohr magneton, and H is magnetic field strength.

Mott-Schottky curves can be used to determine the type of semiconductor, obtain the flat-band potential of the material, and reflect the density of the majority carrier in the sample. The relationship between the physical quantities follows the following equation:

$$\frac{1}{C^2} = \frac{2}{Ne\varepsilon\varepsilon_0}\left(E - E_{FB} - \frac{kT}{e}\right) \tag{2}$$

Where C is interfacial capacitance, e is the electron charge, N is the donor densities (cm^{-3}), ε is the dielectric constant of the passive film, ε_0 is the vacuum permittivity ($8.854 \cdot 10^{-14}$ F/cm), k is the Boltzmann constant ($1.38 \cdot 10^{-23}$ J/K), T is the absolute temperature and E_{FB} is the flat band potential. The $\frac{kT}{e}$ is about 25 mV at room temperature, which is usually negligible. The positive slope indicates that both N-CN and HN-CN are typical n-type semiconductors, and further calculation of the inverse of the slope shows that the carrier density of HN-CN is 1.14 times higher than that of N-CN. This result is good evidence that the step of protonated precursor can remove the defects generated in the N_2 atmosphere that are detrimental to the carrier density increase. Moreover, the intercept of the tangent line to the transverse axis is in line with the flat-band potential of the samples, and the similar flat-band potential suggests that they have close conduction band potential, which is consistent with Figure 8d.

Table S1. The elemental analysis of different samples: CN, N-CN, H-CN, and HN-CN

Sample	C (wt%)	N (wt%)	H (wt%)	O (wt%)	C/N (mass ratio)
CN	34.13	62.15	2.01	1.71	0.55
N-CN	34.63	62.78	1.93	0.66	0.55
H-CN	33.18	59.57	2.29	4.96	0.56
HN-CN	33.53	63.04	2.20	1.23	0.53

Table S2. The fractions of various C types for different samples: CN, N-CN, H-CN, and HN-CN

Sample		C1	C2	C3	C4
CN	At %	14.3	2.6	76.4	6.8
	Area	2713.5	491.5	14492.5	1281.7
N-CN	At %	9.5	3.4	45.9	41.2
	Area	1853.3	663.6	8977.4	8051.9
H-CN	At %	11.2	2.2	82.1	4.5
	Area	2778.8	556.1	20427.9	1126.0
HN-CN	At %	14.4	3.1	77.9	4.6
	Area	3729.3	802.9	20222.6	1186.4

Table S3. The fractions of various N types for different samples: CN, N-CN, H-CN, and HN-CN

Sample		N1	N2	N3	N4	(N1+N2)/N3
CN	At %	48.8	32.7	12.9	5.7	6.32
	Area	16022.4	10734.3	4232.9	1866.0	
N-CN	At %	36.2	37.0	20.3	6.4	3.60
	Area	13360.1	13641.4	7496.1	2362.2	
H-CN	At %	59.4	22.1	12.2	6.3	6.65
	Area	28864.1	10737.7	5953.9	3062.5	
HN-CN	At %	55.2	24.1	14.5	6.2	5.47
	Area	26831.2	11689.7	7042.0	3004.2	